Woods, B., & Friswell, M. (2016). Spiral pulley negative stiffness mechanism for passive energy balancing. Journal of Intelligent Material Systems and Structures, 27(12), 1673-1686. DOI: 10.1177/1045389X15600904

Spiral pulley negative stiffness mechanism for passive energy balancing

Benjamin KS Woods[1] and Michael I Friswell[1]

Abstract

This paper discusses the development, analysis and testing of a mechanism designed to passively balance the energy requirements of mechanical systems and smart structures in order to reduce the size and weight of their actuation systems and to minimize the associated energy consumption. This passive energy balance is achieved by coupling a negative stiffness mechanism to the positive stiffness of the mechanical system being driven, thereby creating a net zero stiffness system which can be actuated with minimal energy requirements. The negative stiffness mechanism proposed here uses a cable spooling around a spiral shaped pulley to convert decreasing forces in a pre-stretched linear extension spring into increasing torque output, thereby creating a torsional spring with negative output stiffness. An analytical model of the system was developed, and the geometry of the spiral pulley was optimized for a representative design case. An experimental demonstrator was then built and tested, confirming the ability of the concept to drastically reduce torque and energy required to actuate a representative load.

Keywords

Negative stiffness; kinematics; mechanism; actuation; energy balance

Introduction

Many different types of mechanical systems and smart structures include actuators to overcome internal and external loads and to allow for controlled motion of components. The design of these actuation systems is driven by a number of variables, one of the most fundamental being the distribution of force required over the desired range of motion (or analogously, torque required in a rotary system). Very often when actuators are used to move a load, they are unable to recover the energy spent, and so incur an energy cost for each cycle of

[1]College of Engineering, Swansea University, UK

Corresponding author
Benjamin KS Woods, College of Engineering, Swansea University,
Singleton Park, Swansea SA2 8PP, United Kingdom.
Email: bewoods@gmail.com

operation. Furthermore, the presence of large forces or torques in a system will lead to an associated scaling of the size, weight, and cost of the actuator, which will affect the performance and viability of the overall system. For very simple cases, such as vertical movement of a mass, the forces needed to create motion can be balanced with a simple counterweight. This directly reduces the force/torque and energy which must otherwise be actively generated by the actuator, and allows for a smaller, lighter and cheaper actuator to be employed. Most systems however, do not display a constant force requirement over their operating range. Many systems instead must act against loads which require an increasing amount of effort with increasing displacement; a property known as positive stiffness. The stretching of a spring, bending of a beam, and deflection of an aerodynamic flap are all examples of positive stiffness loads. In order to passively balance the energy requirements of positive stiffness systems such as these, negative stiffness is required.

Positive stiffness, in a structure or in a mechanism, can be characterized as something that requires increasing effort to undergo increasing deformation. Or in other words, something that pushes back with increasing force when moved. Negative stiffness systems have the complete opposite behavior; when you move them, they pull you with increasing force. Negative stiffness systems generate forces (or torques) which tend to amplify any displacement put into them. This is a somewhat counter-intuitive situation, mostly because negative stiffness is not commonly found in either nature or the manufactured world. One interesting exception are the hairs in our inner ears, which have been shown to display negative stiffness characteristics (Martin et al., 2000). Humans, and indeed many other animals, employ negative stiffness in their ear hairs as a way to increase the response sensitivity of the hair, thereby providing increased hearing capability. Despite their scarcity in nature, negative stiffness structures and systems are fairly well-established concepts in the literature, and are an active area of research for a variety of reasons. They have been shown to have unique vibration isolation properties (Lee et al., 2007; Platus, 1999; Le and Ahn, 2011), the ability to exhibit large damping ratios (Lakes, 2001), and can display very large local stiffness (Wang and Lakes, 2004).

The most common mechanism for creating negative stiffness in the literature is a buckled beam under side loading, as shown in Figure 1, which is borrowed from Fulcher *et al.* (Fulcher et al., 2014). A buckled beam will have two stable equilibrium states, shown in Figure 1a as (1) and (3). Application of a side force (F_t in the figure) will allow for movement from one stable state to the other, but in a highly non-linear way. As seen in Figure 1b, the system will initially have high positive stiffness as the curvature of the buckled beam resists movement, but at a certain point the beam softens, and then goes through a region of negative stiffness before returning again to positive stiffness in the vicinity of the other stable equilibrium point. If the displacement is

unconstrained, the region of negative stiffness will cause a sudden snap-through. If instead, the center of the beam is attached to a mechanical system, then the negative stiffness behavior can be made to act on that system. Careful design of the combined system can then provide the vibration isolation, high damping ratios, or amplified local stiffness observed in previous work.(Lee et al., 2007; Wang and Lakes, 2004).

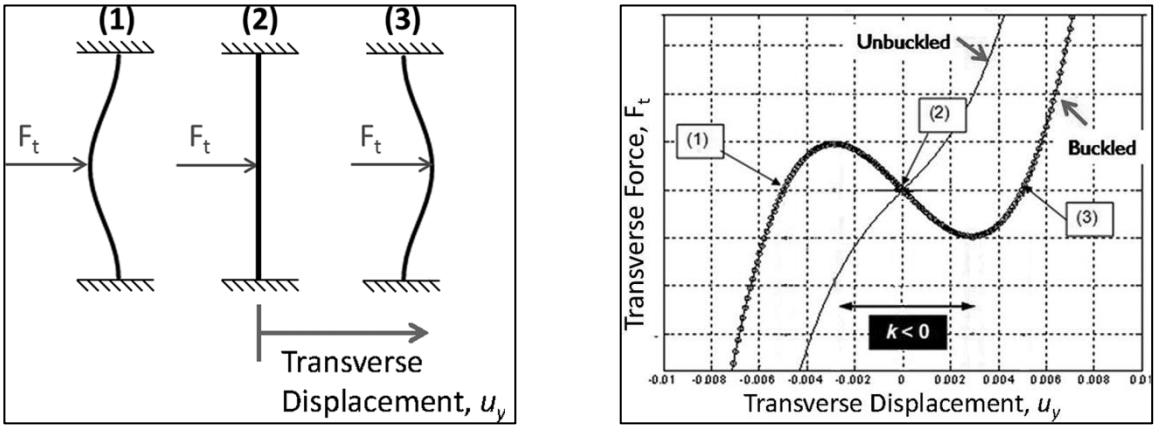

(a) (b)

Figure 1. Buckled beam negative stiffness device from Fulcher *et al.*(Fulcher et al., 2014), a) basic concept and b) localized negative stiffness.

Analogous negative stiffness systems have be made from pre-compressed springs under side loading, as seen in (Wang and Lakes, 2004), or with magnets as in (Carrella et al., 2008). Generally, these systems have behavior similar to that shown in Figure 1b, although of course the particular shapes of the force versus displacement curves are very dependent on the configuration used and its dimensions.

This paper explores an alternative use of negative stiffness. Here the energy stored in a negative stiffness system is used to balance the actuation energy requirements of existing systems which have positive stiffness. The approach will be to couple the two together such that the positive and negative stiffnesses cancel each other to create a net zero stiffness system. In an ideal case, such a design could completely eliminate the loads required to actuate the system. The actuator used to move the system could then be very small with minimal energy consumption. In practice it is impossible to perfectly balance stiffness (particularly in systems where the baseline positive stiffness may change over time or with operating conditions), and the inevitable presence of friction means that the actuation requirements will never be zero. However, any achievable reductions in the forces or torques required will likely lead to reduced actuator weight, size, cost, and running costs. These savings must of course be balanced against the weight, size and cost added by the negative stiffness system itself. To achieve a net system benefit, it is desirable to have a simple negative stiffness mechanism with as high a specific energy (energy stored divided by mass) as possible. This is particularly true in applications for

the transportation industries (aerospace, automotive, rail, etc), where the mass of any devices added will most likely negatively affect the performance of the vehicle.

The use of negative stiffness for passive energy balancing has been proposed in previous work on morphing aerostructures. Morphing aircraft, which can be considered a form of smart structure, seek to provide large changes in the shape of aircraft components to allow for optimized aerodynamic performance over a range of operating conditions (Barbarino et al., 2011;Weisshaar, 2006) . A common approach to providing this change in shape is to elastically deform structural components, twisting of a wing for example (Pendleton et al., 2000; Monner et al., 2008; Chen and Chopra, 1997) or bending of an airfoil's camber (Kudva, 2004; Daynes and Weaver, 2011; B KS Woods et al., 2014), often with the use of smart materials as the actuators. These compliance based approaches have the benefit of smooth and continuous shape change and can be mechanically simple, but often suffer from high energy requirements due the elastic strain energy which must be put into the structure to deform it. This can lead to excessive weight penalty from the actuation system needed; thereby compromising the net effectiveness of the morphing structure.

Two previous examples of negative stiffness mechanisms used to balance energy in morphing applications exist in the literature. Clingman and Ruggeri proposed a negative stiffness energy balancing approach for use on wings or helicopter blades employing active twist (Clingman and Ruggeri, 2004). This work used a variation of a snap-action mechanism (Sclater, 2011), which are also called toggle or bi-stable mechanisms, as seen schematically in Figure 2. The kinematics of the connection between a spring, linkage, and rotating output shaft create a region of negative stiffness. In typical applications of a snap-action mechanism, such as a toggle switch, this region of negative stiffness is what causes the device to snap through to its second equilibrium point. Clingman and Ruggeri used it instead to provide passive energy balance for a morphing twist wing. Given the smaller angles of rotation desired for the active twist concept (±15°), the somewhat limited range of rotation achievable with this design was appropriate. This particular application suffered from significant friction however, due in part to the implementation of the required linear sliding element. Figure 3 shows the experimentally measured performance of this device, with the actuation torque requirements of the combined system (load spring plus negative stiffness mechanism) being shown for both the analysis (solid line) and the measurements (diamonds). Note that the measured torque is significantly higher than that predicted due to friction and perhaps additional unmodeled effects. Despite this, the device was able to provide up to a roughly 50% reduction in actuation torque compared to the load without negative stiffness mechanism.

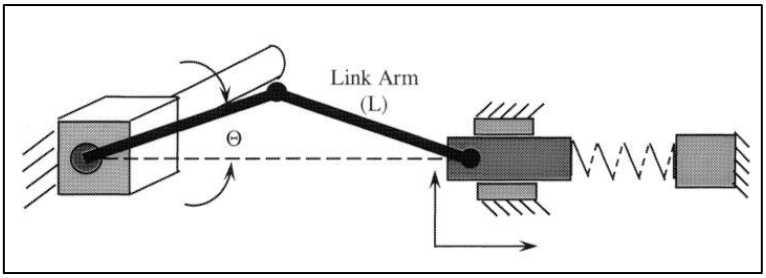

Figure 2. Pre-compressed spring negative stiffness mechanism from (Clingman and Ruggeri, 2004).

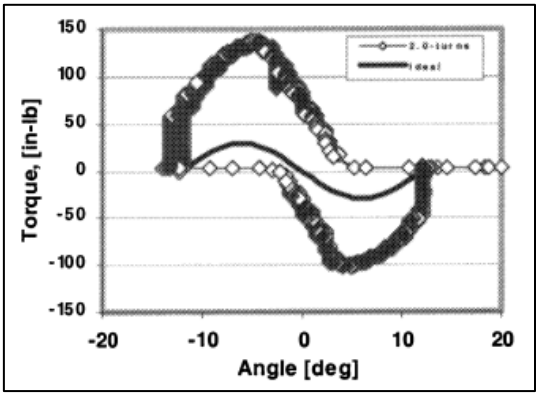

Figure 3. Experimentally measured torque requirements of active twist rotor energy balancing system from (Clingman and Ruggeri, 2004).

Another example of passive energy balancing can be found in the work of Lachenal, Daynes, and Weaver (Lachenal et al., 2013), who developed a negative stiffness mechanism composed of curved strips of carbon fiber composite which were straightened and restrained to create a multi-stable structure with a region of negative torsional stiffness. This negative stiffness mechanism was then combined with a warp twist morphing wind turbine blade tip (which exhibited positive structural stiffness) as seen in Figure 4 to create a structure with near zero stiffness capable of ±5° of spanwise twist variation.

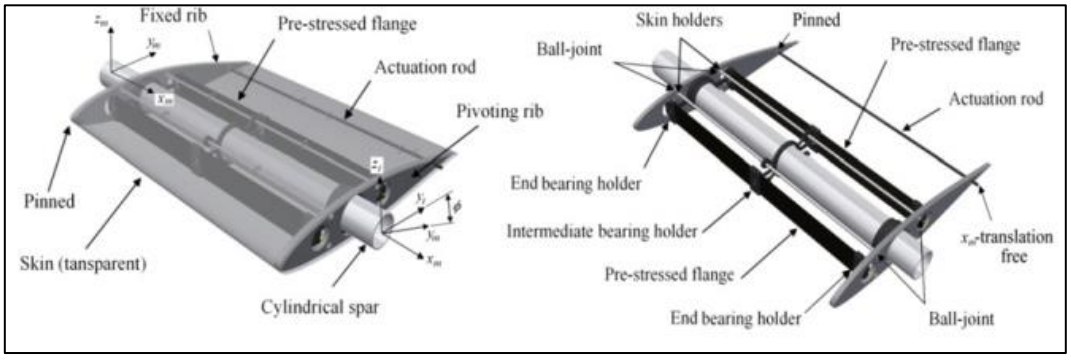

Figure 4. Wind turbine variable twist system employing a negative stiffness mechanism for passive energy balance from (Lachenal et al., 2013).

The torque required to rotate versus rotation angle data for this device is shown in Figure 5, and it can be seen from the experimental data that the negative stiffness mechanism does an effective job of balancing the

skin warping stiffness over the desired operating range. Using this torque data, it is possible to estimate the energy stored in the negative stiffness mechanism as being on the order of 0.08 Nm.

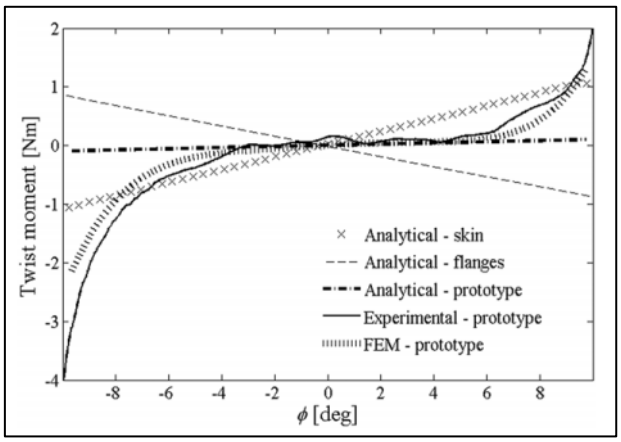

Figure 5. Torque versus rotation requirements for wind turbine blade variable twist system – the flanges are the negative stiffness element, from (Lachenal et al., 2013).

A related concept is the use of precompression of piezoelectic bender actuators as a way to increase their achievable output displacement and force levels (Lesieutre and Davis, 1997). This approach takes advantage of the negative stiffness behaviour of the preloaded beam to reduce the inherent bending stiffness of the elments in the bender actuator, and to thereby reduce the energy the peizos must put in to bend to actuator. This concept has been experimentally validatied and applied to the camber morphing airfoil sections and flight tested on a small scale UAV (Vos et al., 2007).

Beyond the three examples above, work to date has not widely explored the potential of negative stiffness systems to serve as passive energy balance mechanisms, either within morphing aircraft applications or more generally. This is possibly due to the somewhat low levels of force and displacement (which combined represent energy) achievable from existing systems, particularly with respect to their size and mass. In the case of buckled-beam systems, snap-action mechanisms, and the curved strip device of Lachenal, Daynes, and Weaver, the negative stiffness effect exists only over a specific region of the displacement range, which is typically small relative to the overall size of the device. Furthermore, the magnitude of the negative stiffness is constantly changing as the structure moves through regions of positive stiffness, then negative, and then back again to positive stiffness. This behavior complicates effective matching of the force/torque required. The limitations of existing negative stiffness systems have therefore restricted the range of appropriate applications.

If instead there was a system which displayed nearly constant magnitude negative stiffness over a large range of motion and which had the ability to generate substantial forces/torques (relative to its size and weight), then the potential application areas of passive energy balancing would grow considerably. Furthermore, if the

negative stiffness were scalable and highly tailorable to allow, for instance, for non-linear stiffness or force offsets, then an engineer would have a lot more design freedom and the ability to customize solutions for different conditions. With these desired characteristics in mind, the spiral pulley negative stiffness mechanism will now be introduced.

Spiral pulley negative stiffness concept

This section will present the Spiral Pulley Negative Stiffness (SPNS) mechanism used in this work to provide large magnitude torques and rotations for passive energy balancing. The basic concept uses a spiral pulley with cable spooling to convert axial force and linear motion in a pre-stressed extension spring into torque and rotary motion in a manner which provides a large degree of control over the transformation kinematics. By tailoring the shape of the spiral pulley, the device can be made to generate a wide range of output load versus deflection shapes; including decreasing torque, increasing torque (the "negative stiffness" of interest here) or even constant torque. This range of functionalities is achieved by controlling how quickly the moment arm at which the force in the cable acts is ramped up. If the ramping up is gradual, then the decreasing force available from the spring will still result in a decreasing torque output, albeit with a modified shape of its output torque versus rotation behavior, which is referred to herein as a load line. If the increasing moment arm is perfectly matched to the decreasing force available, then a constant torque output load line can be created. If, however, the moment arm is increased even more rapidly the torque output will in fact grow with rotation. It is this configuration which effectively creates negative stiffness, allowing the spring to behave like an actuator and put energy into the driven system. One important difference between this negative stiffness mechanism and an actuator is the fact that the SPNS device is passive and does not require recurring external energy input in the form of electricity, fuel, pressurized fluid, or heat as an actuator would.

Furthermore, with careful selection of the spiral shape and optimization of the design parameters, the output load line of the SPNS can ideally be made to exactly match the requirements of the load, eliminating the torque required to move the load. Since the stiffness of the load is itself a form of elastic energy storage, the combined system can be thought of as having continuous torque equilibrium and constant total energy (ignoring friction and other losses). Motion of the output occurs freely because energy can be transferred from the SPNS mechanism to the load, and back, with no change to the total amount of energy in the system. It it important to note that the resulting near-zero stiffness system would not necessarily be intrinsically stable, as the output position would be free to move considerably under small variations in load. It is intended that stability would be

provided in any real world system through other features, such as non-backdriveablility in the actuation system, friction, brakes on the output, etc. This initial work will not consider stability in any further detail, but it is an important aspect of the design of such systems that will be critical to study further in future work.

The operating principle of the SPNS mechanism is shown schematically in Figure 6, with the components in blue denoting the initial state and the components in red showing the device after rotation of the pulley through the angle, δ. Note that as the pulley rotates the spring gets shorter but the offset between the cable and the center of rotation gets larger. In order to show the negative stiffness behavior of this mechanism, and to allow for the design of a system to passively balance a given load, we must derive the underlying kinematics and torque behavior of the device. The spiral pulley mechanism was initially developed in previous work by the authors where a pneumatic actuator was used instead of the drive spring shown in Figure 6 (B K S Woods et al., 2014). The intention of this previous study was to modify the output load line of the actuator to improve its mechanical conversion efficiency when driving compliance based morphing aircraft systems. The replacement of the active component with a passive spring takes the concept one step further to create a system with both a large degree of control over the kinematics and the ability to passively balance the energy required to drive a load.

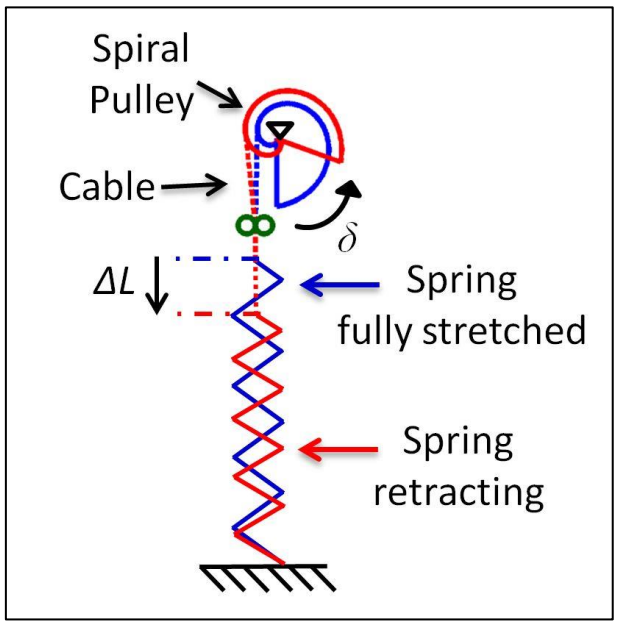

Figure 6. Spiral pulley negative stiffness mechanism operating principle

Spiral pulley performance analysis

The analysis methodology for the spiral pulley negative stiffness mechanism is considered next. The kinematics of the spiral pulley and spooling cable are first derived. The equations for torque output from the

drive spring acting through the spiral pulley are then given. The linear torsional stiffness of the representative load to be driven by the SPNS mechanism is created with a linear extension spring acting through a constant radius cable spooling pulley. The equations for this load torque are derived, and the resulting total system torque for quasi-static operation will be given.

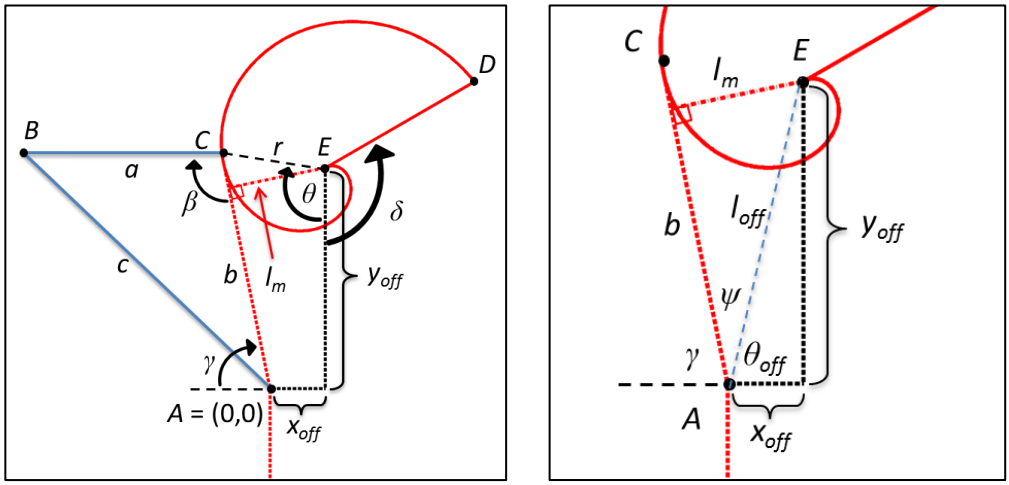

(a) (b)

Figure 7. Spiral pulley geometry, (a) overview, (b) moment arm detail

The detailed geometry definition of the spiral pulley is shown in Figure 7. In order to determine the length of the moment arm, l_m, and the amount of drive spring displacement, ΔL, which occurs due to rotation of the spiral pulley about point E by the angle δ, the kinematics can be derived as follows.

First, we prescribe an exponential radius profile of the spiral pulley in polar coordinates about point E:

$$r_s = r_0 + k_1 e^{k_2(\theta+\delta)} \tag{11}$$

Note that although the variation in radius used here is exponential (with a constant offset), any profile could be adopted. High order polynomial or trigonometric formulations, for example, could potentially better match different types of desired force profiles.

The Cartesian coordinates (with the origin at point A) of any point C along the spiral profile can then be found from:

$$x_C = x_{off} - r_s \sin(\pi - \theta) \tag{12}$$
$$y_C = y_{off} + r_s \cos(\pi - \theta) \tag{13}$$

The length of cable, b, between point C and the origin is equal to:

$$b = \sqrt{{x_C}^2 + {y_C}^2} \tag{14}$$

The arc length, S, of the cable wrapped around the pulley from point C to the cable anchor point, D, can be found from the general form of the arc length formula:

$$S = \int_{\theta(C)}^{\theta(D)} \sqrt{r^2 + (\frac{dr}{d\theta})^2} d\theta \; = \int_{\theta(C)}^{\theta(D)} \sqrt{(r_0 + k_1 e^{k_2(\theta+\delta)})^2 + (k_2 k_1 e^{k_2(\theta+\delta)})^2} d\theta \tag{15}$$

The total length of cable, L_c, is then equal to

$$L_c = b + S \tag{16}$$

The portion of cable that initially lies between point *A* and the drive spring (as seen in Figure 6) is not relevant for this analysis since its length is essentially constant, and therefore makes no contribution to the change in length of the drive spring. Instead, the change in drive spring length can be found by subtracting the total cable length evaluated at the current pulley rotation angle, δ, from the total cable length at the initial pulley rotation angle, δ_0, which for this analysis is zero.

$$\Delta L_d = \; L_c|_{\delta_0} - L_c|_{\delta} \tag{17}$$

The moment arm, l_m, at which the force in the cable acts is defined as the length of the vector perpendicular to vector $\overline{AC}$ which passes through point *E*. To find this it is necessary to first determine the angle that vector $\overline{AC}$ makes with the horizontal axis, defined as γ in Figure 7. This is done using the law of cosines for the triangle ABC. The coordinates of point *B* will be:

$$x_B = x_C - a \tag{18}$$

$$y_B = y_C \tag{19}$$

where *a* is a fixed, arbitrary length, taken to be 50 mm for this analysis. The length *c* of vector $\overline{AB}$ is equal to:

$$c = \sqrt{{x_B}^2 + {y_B}^2} \tag{20}$$

With *a*, *b*, and *c* now known, the law of cosines can be applied to find the angle β:(Hazewinkel, 2001)

$$\beta = \cos^{-1}\left[\frac{a^2+b^2-c^2}{2ab}\right] \tag{21}$$

From the geometry of vector $\overline{AC}$:

$$\gamma = \pi - \beta = \pi - \cos^{-1}\left[\frac{a^2+b^2-c^2}{2ab}\right] \tag{22}$$

The angle of the pulley rotation point relative to the origin, θ_{off}, is found from:

$$\theta_{off} = \tan^{-1}\left(\frac{y_{off}}{x_{off}}\right) \tag{23}$$

The moment arm angle, ψ, in Figure 7b can now be derived given ψ and θ_{off}:

$$\psi = \pi - \gamma - \theta_{off} \tag{24}$$

The length of vector $\overline{AE}$, l_{off}, is equal to:

$$l_{off} = \sqrt{{x_{off}}^2 + {y_{off}}^2} \tag{25}$$

We can now solve for the moment arm;

$$l_m = l_{off} \sin \psi \tag{26}$$

Equations (17) and (26) have been derived for any point *C* on the profile of the spiral pulley. However, in practice there is only one point that is physically relevant to the unspooling action of the pulley at a given δ, and that is the point at which the straight portion of the cable $\overline{AC}$ leaves tangent to the spiral pulley surface.

The point of tangency occurs when the point *C* has the minimum corresponding angle γ. The value of theta at the tangent point, $\theta_{min\,\gamma}$, can be solved for by differentiating Equation 21 with respect to θ and setting equal to zero:

$$\frac{d\gamma}{d\theta}|_{\theta_{min}\,\gamma} = 0 \tag{27}$$

After solving for $\theta_{min\,\gamma}$ for a given δ, the corresponding ΔL_d and l_m can be found from Equations 17 and 26.

The drive spring is stretched by an initial amount L_0 so that it may store elastic energy. The force in the drive spring, F_d, can therefore be found from:

$$F_d = K_d(L_0 - \Delta L_d) + F_{off,d} \tag{28}$$

Where K_d is the drive spring constant, and $F_{off,d}$ is the force offset present in the spring. This force offset is a result of the manufacturing method used with extension springs of the type implemented here, and appears as an initial non-linear, high stiffness region in the spring's extension before the nominal spring stiffness is achieved. As this force can be considerable, it is important to include it in the analysis. Experimental characterization of the springs used here presented in the Design Case section below shows typical force offset behavior. The torque resulting on the spiral pulley from the drive spring acting at its current moment arm will be:

$$T_d = F_d l_m \tag{29}$$

The load spring acts on the system through a constant radius spooling pulley, and so its analysis is simpler. The load spring is installed at its resting length, but again has a force offset, $F_{off,l}$, so its force at a given length can be found from:

$$F_l = K_l \Delta L_l + F_{off,l} \tag{30}$$

The change in length of the spring due to rotation of the constant radius spooling pulley (which is fixed to the spiral pulley and therefore experiences the same rotation, δ) can be found form the circular arc length formula:

$$\Delta L_l = r_l \delta \tag{31}$$

where r_l is the constant pulley radius. The load torque is then equal to:

$$T_l = F_l r_l = K_l r_l^2 \delta + r_l F_{off,l} \tag{32}$$

The evolution of the load and drive torques as the pulleys rotate is the focus of this analysis, and the equations above provide a full description of the quasi-static behavior of the SPNS mechanism. They do not however, tell the designer what the geometry of the spiral pulley should be to provide the best performance for a given design case. To accomplish that, we shall now investigate a representative design case and use an optimization routine to design the geometry.

Design case

In order to show the efficacy of the passive energy balancing concept, it is useful to consider a particular design scenario. Given the broad scope of applications envisioned for this mechanism, this design scenario will be generic. The system proposed here is intrinsically scalable, limited mainly by the availability of the required components, which include drive springs, bearings, and cables/cordage of different sizes. Given that these simple elements are ubiquitous and already manufactured over a very broad range of scales and load ratings, in should be possible to apply this concept quite widely. The intention with this initial study will therefore be to show the large rotation range and considerable energy storage achievable in a moderately sized table top demonstrator.

The linear extension spring used for the load is the most important parameter in the sizing of this system, since it represents the energy required to be balanced by the negative stiffness system. The output rotation range was prescribed to be $0 \leq \delta \leq 250°$ to show the ability of this approach to widen the design space over existing concepts, which have typically been limited to less than ±15° of rotation range. A target load stiffness of 1000 N/m was chosen, and a commercially available spring was found with a measured spring constant of K_l = 1050.8 N/m (Ashfield Springs Ltd. part number S.100), which was deemed suitable. Figure 8 shows the force versus extension behavior of the load spring used here, and an initial non-linear range can be seen which effectively creates a force offset of 22 N to the linear range of the spring's motion. The constant radius of the load spooling pulley was fixed to 25 mm, which gives a resultant torsional stiffness of 0.0114 Nm/deg.

Also shown in Figure 8 is the drive spring used in this analysis, a softer extension spring (K_d = 590.7 N/m, Ashfield Springs Ltd. part number S.119) which is capable of larger extensions due to its lower stiffness and longer resting length (229 mm versus 178 mm). Note again the force offset, which is even larger in this case at 33.3 N. The selection of this drive spring was part of the optimization process, as discussed in detail below.

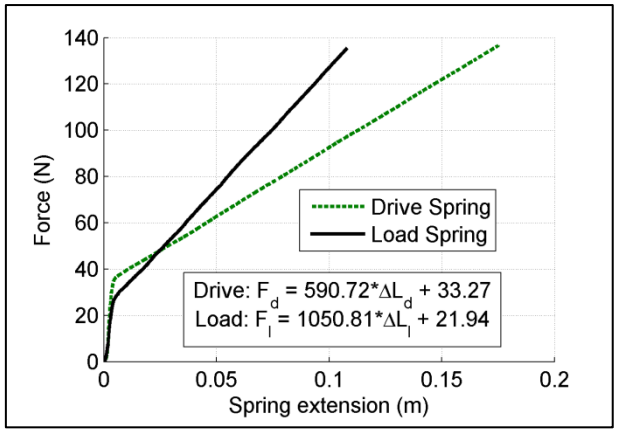

Figure 8. Force versus extension behavior of the load and drive springs, with equations for the linear fits (which exclude the initial non-linear region)

Geometry optimization

In order to maximize the performance of the energy balancing system, the geometric parameters of the spiral pulley were optimized using the Firefly single objective metaheuristic optimization algorithm (Gandomi et al., 2011). The objective function used was designed to make the torque available from the SPNS mechanism match as closely as possible that required by the load over the entire desired operating range. To accomplish this, an absolute energy difference metric, *J*, was derived which integrates the absolute magnitude in torque difference between the SPNS mechanism and the load over the prescribed rotation range, according to:

$$J = \int_0^{\theta_{max}} |T_d - T_l| \, d\theta \tag{33}$$

The upper and lower bounds set for the design variables are given in Table 1. Note that these bounds are fairly open, as it was desired to not arbitrarily restrict the design space. The spring rate of the drive spring needed special consideration, as the drive spring was to be chosen from a range of commercially available springs. Initially, drive spring rate was allowed to be a continuous variable within the optimization, with bounds set by what was available from the chosen supplier (Ashfield Springs Ltd.). After running the optimization, the available spring with the closest matching spring rate was chosen, and the analysis was rerun for the actual spring rate to ensure good performance. In a similar way, the initial extension of the drive spring is also limited by the maximum extension of the spring, which of course depends on the particulars of each spring. The optimized value was checked against the maximum for the spring with the closest spring rate, and in this case the optimal value was less than the maximum. Alternatively, this optimization could have been performed using discrete values for drive spring rate and initial extension taken from a list of available springs, as the firefly algorithm can handle such discrete variables without difficulty.

Table 1. Design parameters for spiral pulley optimization

Parameter	Lower Bound	Upper Bound	Optimized Value	Units
Initial radius, r_0	-10	10	-0.795	mm
Pre-exponent term, k_1	-0.05	0.05	0.00257	–
Exponent term, k_2	0	1	0.494	–
Drive spring extension, L_0	0.02	0.25	0.218	m
Drive spring rate, K_d	100	1000	611.0	N/m

For a given potential geometry (known as a "firefly" for this algorithm), a sweep of spiral pulley rotation angles was analyzed, with the drive torque available and load torque required determined for each angle. The objective function (Equation 33) was then evaluated using the resulting evolution of torques with delta. A total of 200 fireflies were run for 60 generations, and the objective function was tracked to ensure convergence. Repeated runs showed consistency in the converged solution, with slight variations as expected given the use of a random search component within the optimization algorithm. The resulting optimized parameters are shown in Table 1. Note that, as explained above, the optimal value of drive spring rate is slightly different from that of the chosen spring (590.7 N/m, as seen in Figure 8).

The optimized spiral pulley shape is shown in Figure 9, along with the constant 25 mm radius load pulley. Note that the end of the spiral pulley has been truncated to prevent interference with the test rig during rotation. The portion of the spiral cut off is not actually used over the 250 degree rotation range specified for this demonstrator, and so the performance is unaffected. Also visible in the figure are two holes (besides the central shaft hole) through which dowel pins were run to provide torque transfer between the two pulleys.

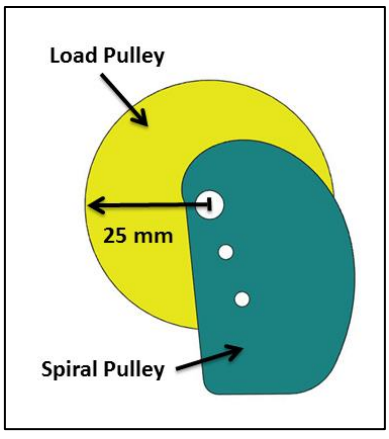

Figure 9. Optimized spiral pulley geometry

The performance predicted for this spiral pulley geometry shows good, if not perfect, matching of the torque requirements. In Figure 10 can be seen the evolution of torque with rotation for the drive and load springs, and the resulting net torque. The results for both the optimal value of drive spring stiffness (K_d = 611.0

N/m) and the actual stiffness of the available spring (K_d = 590.7 N/m) are shown. While the spiral pulley is not quite able to convert the positive linear drive spring stiffness into a perfectly linear negative output stiffness, the resulting net torques are indeed significantly lower than the load by itself. It is possible that more complex formulations of the spiral pulley radius distribution would allow the optimizer to find solutions with less curvature in the output, and therefore even lower net torques. Nevertheless, the fairly simple radius formulation chosen here and the corresponding predicted performance is adequate for the purposes of this initial demonstration. Note that the results for the optimal and available spring stiffnesses are very similar.

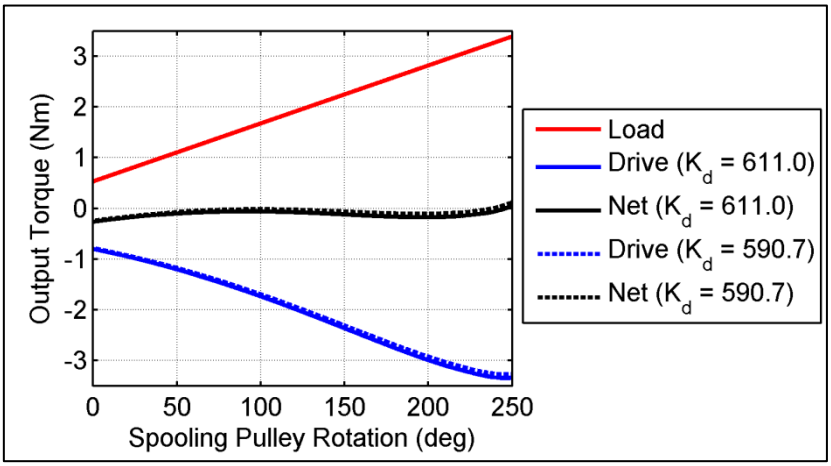

Figure 10. Predicted performance with optimized (K_d = 611.0 N/m) and available (K_d = 590.7 N/m) drive spring stiffnesses

Integration of the torque versus rotation curves gives the mechanical energy required to drive the load, as plotted in Figure 11. By comparing the energy required by the load spring alone to that of the load with the SPNS device attached, the ability of the negative stiffness mechanism to passively balance the load energy can be seen. Indeed, the predicted reduction in total energy required over the 250° spooling pulley rotation angle range is 96%, with energy required reduced from 8.56 Nm to 0.33 Nm. The SPNS device is therefore predicted to be able to store and passively transfer 8.23 Nm of energy.

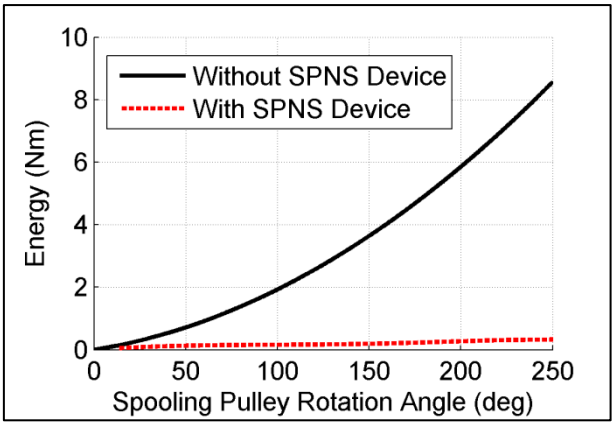

Figure 11. Evolution of predicted energy required to drive load with and without SPNS device

Further insight into the operating principle that allows for such effective reduction of actuation energy requirements can be seen by considering Figure 12. This figure plots the evolution of the force available from the drive spring along with the moment arm at which that force acts at. It can be seen that while the force available from the drive spring does indeed decrease with rotation, the magnitude of the moment arm at which that forces acts increases much faster, leading to a net increase in torque. Note that the force decrease is not linear with rotation. This is a result of the changing pulley radius: as radius increases the amount of cable drawn in for a given change in rotation angle increases, leading to an increasing rate of force loss with increasing rotation.

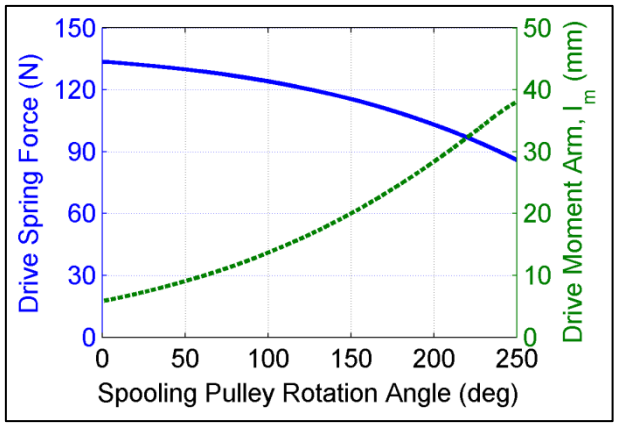

Figure 12. Evolution of drive spring force and moment arm with rotation

Having established the basic operating mechanism of the spiral pulley negative stiffness mechanism, and having shown the promise that it holds for being able to passively balance the energy requirements, we turn now to the experimental validation of the concept's performance.

Experimental test rig

A test rig was built to allow for experimental testing and validation of the SPNS concept and the analysis methods proposed. This test rig was built on a modular frame made from extruded aluminum rails with adjustable brackets mounting the various components. A labeled top view of the completed test rig is shown in Figure 13.

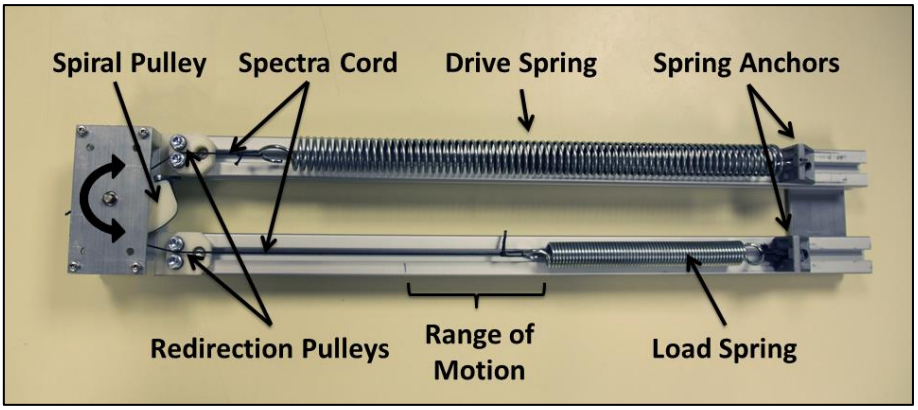

Figure 13. SPNS mechanism test rig

The pulleys were mounted onto a central shaft which was supported by radial bearings set into two spaced plates mounted to the frame through a set of risers, as can be seen more clearly in Figure 14. A contactless angle sensor (Gill Sensors Part #1498-00-068) was installed below the shaft to measure the pulley rotation angle δ directly. The fixed ends of the two springs were mounted to sliding brackets on the frame, which allowed for fine tuning of their resting positions, and which also provided a means of pre-stretching the drive spring. High strength Spectra cordage was run from each spring and wrapped around the corresponding pulley, before being anchored with bolts threaded into the pulleys. The pulleys and several of the ancillary components were 3D printed from acrylonitrile butadiene styrene plastic on a fused deposition modeling printer (HP Designjet 3D Printer model number CQ655A). The offsets between the pulley rotation point and the redirection pulleys for the drive spring, x_{off} and y_{off} in the analysis above, were set to 10 mm and 50 mm respectively to provide sufficient clearance for the pulley. The optimization discussed above took these prescribed values into account.

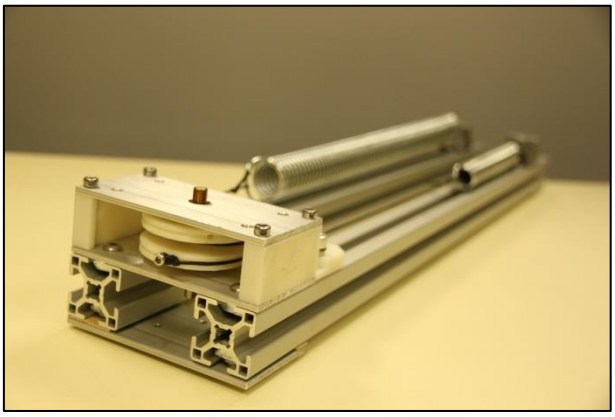

Figure 14. Isometric view of test rig showing pulley mounting

The masses of each component are presented in Table 2. The mass of the mounting frame dominates the total. The frame built here was designed primarily for modularity and simplicity, and therefore is significantly heavier than what would be required in practice. Furthermore, it is likely that many of the functions of the

frame could be served by existing pieces of structure in any real world application, significantly reducing the mass which would be added. The drive spring is the heaviest non-frame component, as is expected given the fact that it must store the energy required. The mass of the load spring is not included in the totals, as this component would be replaced by whatever positive stiffness system the SPNS device was installed in. Given the predicted energy storage of 8.23 Nm, this initial prototype system is expected to have a specific energy storage capacity on the order of 29.50 Nm/kg without the frame mass and 5.17 Nm/kg with it.

Table 2. Component mass breakdown of experimental test rig

Component	**Mass (g)**
Spiral Pulley	7.71
Load Pulley	10.85
Cordage + Anchor Bolts	3.40
Main Axle + Bearings	13.30
Drive Spring	220.9
Load Spring (not it total)	113.5
Redirecting Pulleys + Bolts	22.81
Mounting Frame	1312.3
Total with Frame	1591.3 g
Total without Frame	278.9 g

Once assembled, the test rig was mounted to a material test machine for displacement cycling. As seen in Figure 15, the frame of the SPNS device was mounted to the moving piston of the test machine. The device was aligned such that force could be applied directly to the load spring using a secondary piece of cordage attached to the upper crosshead of the testing machine. The corresponding amount of torque that would have been required if the shaft had been directly driven was found by multiplying the measured force by the known radius of the load pulley. The chosen test method of pulling directly on the load spring, while simple to implement, does have some implications on the measurement of friction in the device, as will be discussed further below. The angle sensor was mounted to the spinning pulley shaft and connected to the data acquisition system of the material test machine. A 500 N load cell was installed between the cordage and the crosshead to record the tension applied to the load spring.

Figure 15. SPNS mechanism installed on material test machine

In order to allow for characterization of the different components of the torques that add up to the net system, the load spring was first tested by itself. This was done with the entire mechanism in place, but with the drive spring tied off in a manner which isolated the force it generates from the pulley shaft and which did not move with extension of the load spring. The load spooling cordage would therefore be slack as the load spring was stretched directly by the supplementary loading cordage attached to the test machine. The SPNS mechanism was then reengaged, and the test rerun such that the test machine would measure the net force required to move the combined system.

Results and discussion

We will now consider the experimentally measured torque and energy profiles and compare them to the predictions from the analysis. Figure 16 shows the experimentally measured and analytically predicted evolution of torque for the device. For the analysis, the load and drive torques are calculated and the net is the difference. In the case of the experiments, the force required to move the load by itself and then the net system are measured and converted into torques about the shaft. The experimental drive torque is then found from the difference. These results show that the spiral pulley negative stiffness concept does indeed allow for drastic reductions in actuation requirements through passive energy balancing. The negative stiffness behavior of the SPNS mechanism is also clearly evident. The maximum torque required to move the load over the entire 250°

rotation range decreases from 3.52 Nm with the SPNS device disengaged to 0.28 Nm with it engaged, a reduction of 92%.

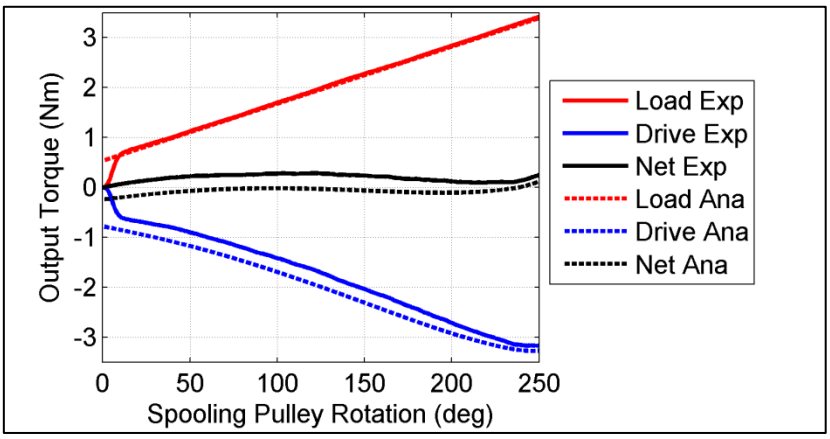

Figure 16. Comparison of experimental (Exp) and analytical (Ana) torques for the SPNS device

There are some details of the torque results in Figure 16 which warrant further discussion. Firstly, it can be seen that the linear fits with force offset used to model the load spring do not properly capture the initial non-linear portion of its behavior. Given that this non-linear range is only a small portion of the output range, this is perhaps an acceptable simplification; certainly so within the context of this initial concept validation. The second aspect to notice is the over-prediction by the analysis of the magnitude of negative torque generated by the SPNS device. There is a resulting offset in both the drive torque and the net torque that diminishes slowly with rotation. It is interesting to note that there is no such offset in the load torque. This is the result of friction in the system and the specific testing method used. As mentioned above, the load spring was stretched directly by the test machine through a supplementary piece of cordage. For this reason, rotational friction present in the device would not be measured when only the load spring was being tested (that is, when the negative torque from the SPNS device was disengaged). However, with the SPNS device engaged, any friction present in the various bearing components would be able to impact the measured forces and calculated torques.

We can consider the effect of friction further by including an empirical correction to the analytical model. If we hypothesize that due to the testing method used, the torque measured in the net system is caused by the force in the drive spring and is therefore proportional to it, then an appropriate friction factor can be empirically fit. By including a frictional torque, T_f, equal to:

$$T_f = \mu_f F_d = 0.0022 F_d \tag{34}$$

into the analytical predictions, the results shown in Figure 17 are obtained, which show considerably better agreement with the experiments. The empirically fit friction coefficient of μ_f = 0.0022 is fairly low, and seems

reasonable given the various friction mechanisms present (shaft rotary bearings, cordage/pulley rubbing, cordage/redirection pulley interaction, etc.).

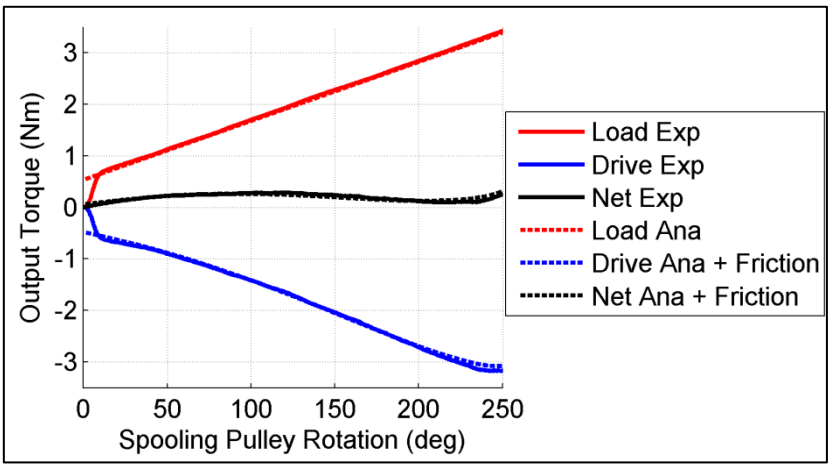

Figure 17. Comparison of experimental (Exp) and analytical (Ana) torques with empirical friction factor

Having established the ability of the purely analytical model to predict the general behavior of the system, and the ability of the augmented model (with empirical friction factor) to quite closely capture the measured performance, we will now consider further aspects of the system using only the experimental results.

By integrating the experimentally measured load torque and net torque curves shown in Figure 16, the energy requirements of the different configurations over the rotation range can be determined. Figure 18 shows these results and the significant reduction in energy requirements provided by the passive energy balancing of the SPNS mechanism is clear. The measured total energy required over the 250° operating range without the SPNS device is 8.61 Nm, but only 0.83 Nm with it engaged. This 90% reduction, while smaller than the 96% predicted by the analytical model (most likely due to friction), is still very significant. The SPNS device is therefore able to passively store and transfer 7.78 Nm of energy, which gives it a specific energy storage of 27.89 Nm/kg for the "active" components (i.e. not including the mass of the test frame). The pulleys and other components could likely be designed to have lower mass, and it is possible that other types of spring could provide even higher specific energy. Carbon fiber springs, with their combination of high elastic modulus and low density (relative to the stainless steel used here) are particularly promising.

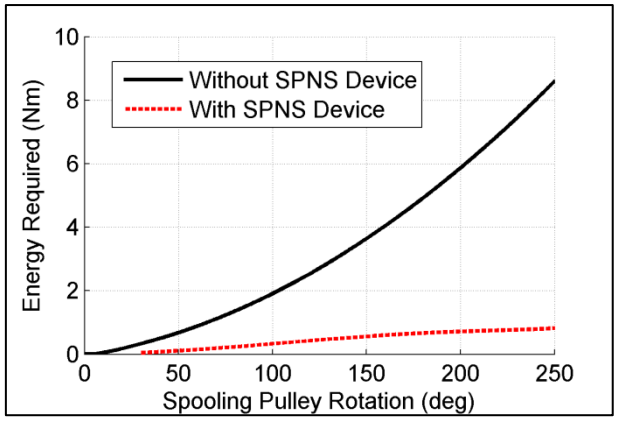

Figure 18. Experimentally measured energy requirements

Finally, we consider the evolution of the reductions in torque and energy required to move the load provided by the SPNS mechanism. In Figure 19a the reduction in torque requirements is shown, and except for during the initial non-linear region of the load spring, the reduction is never less than 80%, and it generally grows with increasing rotation. Figure 19b shows the reduction in energy required with rotation, with similar behavior to the torque reduction, although it fluctuates less since it is an integrated quantity.

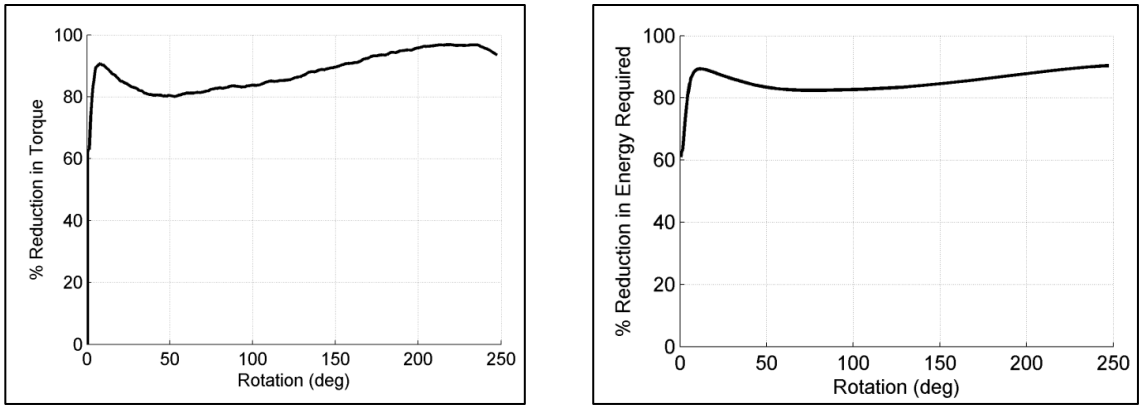

(a) (b)

Figure 19. Reduction in a) actuation torque and b) actuation energy provided by the SPNS device

Conclusions

In summation, this work has introduced a means for passively balancing the actuation requirements of systems displaying positive stiffness through the use of a spiral pulley negative stiffness (SPNS) mechanism. The operating principle of the concept and the motivation for using it were presented, followed by the derivation of an analytical model of the system. The kinematics of the spiral pulley used to convert positive extensional stiffness in a drive spring into negative rotational stiffness were given. The system geometry was then optimized for a representative design case using the firefly meta-heuristic single objective optimization algorithm. The design and testing of an initial concept demonstrator was then shown, and the experimental

results from this device were compared to predictions from the analysis. The viability of the concept was established, and the experiments proved the ability of the SPNS device to drastically reduce both the torque and energy required to actuate the load. The following specific conclusions can be drawn:

- The analytical model of the system provides good predictions of performance, and incorporation of an empirical friction factor improves this considerably.
- The combination of an exponential radius function for the spiral pulley with the firefly optimization algorithm provides good torque matching capability, and the system can be readily adapted to other radius profiles and/or optimization techniques.
- The SPNS device has been experimentally shown to reduce actuation torque requirements by 92% and actuation energy required by 90%, allowing for smaller, lighter and lower cost actuators.
- The configuration tested here has the ability to passively store 7.78 Nm of energy, which is considerable given the simplicity and low mass of the operating components.

Acknowledgements

The research leading to these results has received funding from the European Research Council under the European Union's Seventh Framework Programme (FP/2007-2013) / ERC Grant Agreement n. [247045].

References

Barbarino S, Bilgen O, Ajaj RM, et al. (2011) A Review of Morphing Aircraft. *Journal of Intelligent Material Systems and Structures*, 22(9), 823–877.

Carrella A, Brennan MJ, Waters TP, et al. (2008) On the design of a high-static–low-dynamic stiffness isolator using linear mechanical springs and magnets. *Journal of Sound and Vibration*, EUROMECH colloquium 483, Geometrically non-linear vibrations of structures, 315(3), 712–720.

Chen PC and Chopra I (1997) Hover Testing of Smart Rotor with Induced-Strain Actuation of Blade Twist. *AIAA Journal*, 35(1), 6–16.

Clingman DJ and Ruggeri RT (2004) Mechanical strain energy shuttle for aircraft morphing via wing twist or structural deformation. In: pp. 288–296, Available from: http://dx.doi.org/10.1117/12.538681 (accessed 3 November 2014).

Daynes S and Weaver PM (2011) A shape adaptive airfoil for a wind turbine blade. In: p. 79790H–79790H–11, Available from: http://dx.doi.org/10.1117/12.879208 (accessed 5 December 2014).

Fulcher BA, Shahan DW, Haberman MR, et al. (2014) Analytical and Experimental Investigation of Buckled Beams as Negative Stiffness Elements for Passive Vibration and Shock Isolation Systems. *Journal of Vibration and Acoustics*, 136(3), 031009–031009.

Gandomi AH, Yang X-S and Alavi AH (2011) Mixed variable structural optimization using Firefly Algorithm. *Computers & Structures*, 89(23–24), 2325–2336.

Hazewinkel M (2001) *Encyclopedia of Mathematics*. Springer.

Kudva JN (2004) Overview of the DARPA Smart Wing Project. *Journal of Intelligent Material Systems and Structures*, 15(4), 261–267.

Lachenal X, Daynes S and Weaver PM (2013) A zero torsional stiffness twist morphing blade as a wind turbine load alleviation device. *Smart Materials and Structures*, 22(6), 065016.

Lakes RS (2001) Extreme Damping in Composite Materials with a Negative Stiffness Phase. *Physical Review Letters*, 86(13), 2897–2900.

Lee C-M, Goverdovskiy VN and Temnikov AI (2007) Design of springs with 'negative' stiffness to improve vehicle driver vibration isolation. *Journal of Sound and Vibration*, 302(4–5), 865–874.

Lesieutre GA and Davis CL (1997) Can a Coupling Coefficient of a Piezoelectric Device be Higher Than Those of Its Active Material? *Journal of Intelligent Material Systems and Structures*, 8(10), 859–867.

Le TD and Ahn KK (2011) A vibration isolation system in low frequency excitation region using negative stiffness structure for vehicle seat. *Journal of Sound and Vibration*, 330(26), 6311–6335.

Martin P, Mehta AD and Hudspeth AJ (2000) Negative hair-bundle stiffness betrays a mechanism for mechanical amplification by the hair cell. *Proceedings of the National Academy of Sciences*, 97(22), 12026–12031.

Monner HP, Opitz S, Riemenschneider J, et al. (2008) Evolution of Active Twist Rotor Designs at DLR. In: *Proceedings of the 49th AIAA/ASME/ASCE/AHS/ASC Structures, Structural Dynamics, and Materials Conference*, Schaumburg, IL: AIAA, Available from: http://arc.aiaa.org/doi/abs/10.2514/6.2008-2128 (accessed 5 December 2014).

Nishimura M, Takagi Y and Arai M (2015) *Buckling behavior and atomic elastic stiffness in defective multi-walled carbon nanotube under axial compression*. Key Engineering Materials.

Pendleton EW, Bessette D, Field PB, et al. (2000) Active Aeroelastic Wing Flight Research Program: Technical Program and Model Analytical Development. *Journal of Aircraft*, 37(4), 554–561.

Platus DL (1999) Negative-stiffness-mechanism vibration isolation systems. In: pp. 98–105, Available from: http://dx.doi.org/10.1117/12.363841 (accessed 3 November 2014).

Sclater N (2011) *Mechanisms and Mechanical Devices Sourcebook, 5th Edition*. 5 edition. New York: McGraw-Hill Professional.

Vos R, Barrett R, Breuker R de, et al. (2007) Post-buckled precompressed elements: a new class of control actuators for morphing wing UAVs. *Smart Materials and Structures*, 16(3), 919.

Wang YC and Lakes RS (2004) Extreme stiffness systems due to negative stiffness elements. *American Journal of Physics*, 72(1), 40–50.

Weisshaar TA (2006) *Morphing Aircraft Technology - New Shapes for Aircraft Design*.

Woods BK, Bilgen O and Friswell MI (2014) Wind tunnel testing of the Fish Bone Active Camber morphing concept. *Journal of Intelligent Material Systems and Structures*, 1045389X14521700.

Woods BKS, Friswell MI and Wereley NM (2014) Advanced Kinematic Tailoring for Morphing Aircraft Actuation. *AIAA Journal*, 52(4), 788–798.